NANOSCALE PATTERNING OF METALLIC SURFACES WITH LASER PATTERNED TOOLS USING A NANOIMPRINTING APPROACH

Paul Braun[1], Philipp Grützmacher[2,3], Leonie Frohnapfel[1], Frank Mücklich[3], Karsten Durst[1]

[1] Physikalische Metallkunde, Technische Universität Darmstadt, Darmstadt, Germany
[2] Department of Engineering Design and Product Development, TU Vienna, Wien, Austria
[3] Department of Functional Materials, Saarland University, Saarbrücken, Germany

Abstract

In this study, we demonstrate that metallic substrates with a nanocrystalline grain size can be structured down to the micro- and nanometre range during a room temperature nanoimprinting process. WC-Co hard metal dies are patterned by Direct Laser Interference Patterning (DLIP), generating an array of separated asperities with a height of 4.7 µm and a spacing of 11.3 µm. Additionally, Laser Induced Periodic Surface Structures (LIPSS) with a spacing of 500 nm are formed as a hierarchical substructure. The patterned dies can be used to deform metallic substrates due to their high hardness. For structure replication, the WC-Co tool is pressed onto a nanocrystalline CuZn30 model alloy at room temperature. The pattern transfer process from the hard metallic tool to the nanocrystalline alloy is discussed in detail: At low contact pressures, the asperities on the tools act as single contact points, leading to the formation of separated dimples with a depth of up to 0.8 µm in the nanocrystalline alloy. At high contact pressures, the tool pattern, including the LIPSS is almost completely transferred to the substrate. The formed asperities protrude out of the surface, with a height to width aspect ratio of 0.4. It is thereby demonstrated, that plastic flow processes during the imprinting of nanocrystalline alloys allow for the replication of the DLIP tool pattern, even down to nano-scaled LIPSS. The imprinted array of surface asperities exhibits hydrophobic properties, due to a combined topographical and chemical influence on the wetting behaviour.

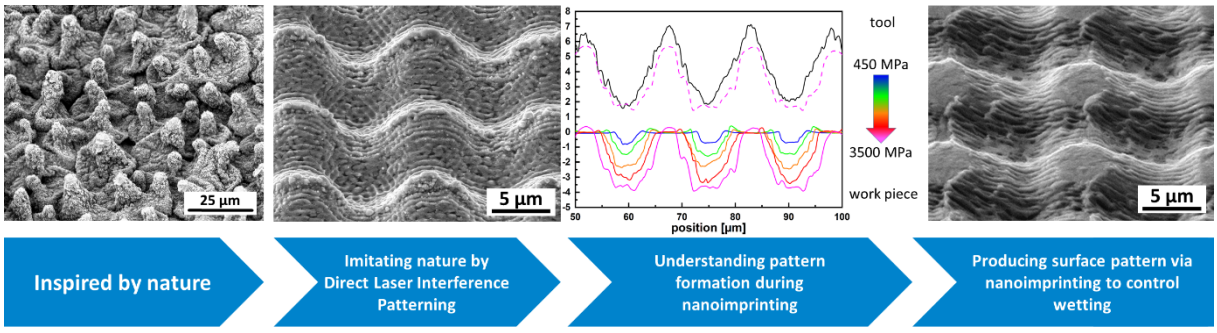

Keywords

Nanoimprinting; Direct Laser Interference Patterning; Wetting; Ageing; Coining; Surface Patterning

1. Introduction

Metallic surfaces can be easily structured with metal forming processes like coining or imprinting at room temperature; however, the available structure size is limited to the sub millimetre regime, strongly depending on the grain size of the material [1, 2]. For many applications, it is necessary to further reduce the length scale of structure features down to micro- or nanometre ranges. In this context, surface patterns on metals (i.e., periodic or random repetition of single surface structures) have shown to be capable of influencing the tribological [3–7] and wetting properties [6, 8–12]. Depending on the patterns' design, wetting, for instance, can be modified from superhydrophilic to superhydrophobic, or even omniphobic behaviour [11–16]. Besides that, heat transfer during boiling [17, 18] or even an improvement of the osteoblast density on dental implants out of titanium [19] can be significantly influenced by modifying the surface.

To form surface patterns onto metals on various length scales, different techniques can be applied, including electromechanical micromachining [20] and vibration-assisted cutting [21] for larger scales, as well as lithography [22] and focused-ion-beam-milling [23] for structures in the dimensions of nanometre and up to micrometre. These techniques are, however, non-continuous processes and cannot be easily upscaled for the patterning of metallic surfaces for industrial application. In the meantime, nanoimprinting has not only shown first successes in nanometre-scale patterning, but is also a promising method for the future of large-area surface patterning. Originally, nanoimprinting lithography was developed for patterning soft polymers above their glass transition temperatures [24, 25] using a micromachined Si-die. Further research allowed nanoimprinting on conventional metals like aluminium, copper, and stainless steel using a silicone tool with structure sizes between 2 µm and 200 µm [26]. For application on metallic materials, the grain size with respect to the structure size will greatly determine the plastic transfer of the tool geometry onto the substrate. Wang et al. [27] showed that for grain sizes in the range of the structure width, only a limited transfer of the tool pattern onto the substrate could be achieved. Furthermore, grain sizes between 23 and 490 µm have been investigated and a minimum ratio of cavity width to grain size of 2.4 with lowest mould filling ability was observed [28]. The metallic nanoimprinting process was further developed by Durst et al., Ast et al. and Braun et al. [29, 30] downscaling the tool structure sizes down to 300 nm

and strongly reducing the grain size to the nanocrystalline regime. Coarse grained materials with a low yield stress showed only a limited pattern transfer and, furthermore, the imprinting would not lead to protruding surface asperities, but rather the formation of dimples in the surface [31]. For ultrafine grained and nanocrystalline metals produced by severe plastic deformation, they demonstrated, that structure sizes of 300 nm with an aspect ratio of 1.1 could be achieved in a single contact nanoimprinting experiment. Nanoimprinting studies so far have been performed using FIB produced flat-ended punches with diameters in the range of 1 - 40 μm. These single contact experiments cannot be easily up-scaled for large area patterning.

Large area patterning based on plastic deformation requires tools, which are strong enough and have a high fracture toughness. Additionally, for many applications small structures are relevant, which is why the tools have to be patterned down to the micrometre regime. Here laser surface patterning offers the unique possibility to pattern larger surface areas on a wide variety of materials and is one of the fastest growing surface patterning methods. This method provides fast, contactless and therefore wear-free processing, as well as a wide range of possible pattern designs [32]. Creating small structures with sizes ranging down to the nanometre scale (< 100 nm) in a very productive way (up to patterning speeds of ~1 m^2/min), especially Direct Laser Interference Patterning (DLIP), has shown to be a promising tool in the past [33, 34]. DLIP is based on the interference of two or more highly energetic laser beams on the substrate surface, resulting in the formation of periodic patterns with a defined long-range order [34, 35]. The patterns' shape is defined by the number of beams, their polarization state, and the phase shift between them [36]. Overlapping two beams, results in the most basic pattern with a one-dimensional line-like shape, whereas three and four beams induce triangular and square arrays of periodic features, respectively [36]. Particularly for ultrashort pulse laser irradiation, in addition to the pattern created by the dedicated interference of the laser beams Laser Induced Periodic Surface Structures (LIPSS) may occur. LIPSS are also (quasi-)periodic structures, which correlate clearly with the laser wavelength and the polarization [37]. It is assumed that they originate from the superposition of the incident laser beam with laser light scattered or reflected at the surface [36, 38] It has been demonstrated that by combining DLIP and LIPSS hierarchical patterns can be generated in a one-step process, which might be interesting, for instance, in wetting applications [37]. Here, it is known that the wettability of the surfaces can be modified to induce super-hydrophobic properties [10]. Laser patterning has been thoroughly investigated with respect to its effects on the tribological properties, e.g., increasing the lubricant lifetime, thus, reducing wear of the work piece [3, 14].

In this study, DLIP is used to micropattern the surface of an imprinting die, which is then used to pattern the surface of a nanocrystalline alloy via an imprinting process. Of particular interest here is the transferability of the tool topography to the substrate and the associated plastic flow processes. It is demonstrated, that DLIP patterns formed on a hard metal WC-Co die, consisting of an array of separated asperities, can be fully transferred to a nanocrystalline CuZn30 alloy including nanoscale surface features. The flow mechanisms during the nanoimprinting process are analysed and it will be shown that depending on the applied contact pressure, different surface patterns (from separated dimples to separated asperities, which protrude out of the surface) can be obtained using the same tool. Therefore, we could show that it is possible to pattern the surface of metallic alloys at room temperature by a simple and fast plastic imprinting process. To demonstrate the changes in the surface properties induced by the surface pattern, contact angle measurements with water are performed. Additionally, the influence of ageing time in dry room air on the wetting behaviour was analysed.

2. Experimental Methods

2.1 Direct Laser Interference Patterning

The surface topography of the nanoimprinting dies was modified using Direct Laser Interference Patterning. For this, a Ti:Sapphire laser source emitting ultrashort laser pulses with a pulse duration of 100 fs at Full Width Half Maximum (FWHM), a centred wavelength λ of 800 nm, and a power of 736 mW (corresponding to a pulse energy of 0.736 mJ) was used. The use of ultrashort laser pulses (pulse duration < 10 ps) allows for creating smaller structures on a wide range of materials with a minimized input of heat into the patterned materials [38]. To create interference of two laser beams the primary laser beam has to travel through an optical setup, shown in Figure 1a. The beam diameter is adjusted by passing an aperture (4.5 mm), which also alters the intensity profile from Gaussian to a near Top Hat. The polarization angle of the laser beam is adjusted perpendicular to the generated pattern orientation by a quarter wave plate. A Diffractive Optical Element (DOE) divides the laser beam into two coherent sub-beams, which are then brought to overlap on the sample surface by a 25 mm lens system with a focal length of 100 mm. The deflection of the beam paths in the optical system has to be kept as low as possible to still allow for interference across the full spot diameter due to the short coherence length of approx. 30 µm in case of 100 fs laser pulses. When the two beams overlap, they interfere and a line-like sinusoidal intensity distribution results, which is illustrated in

Figure 1b. The periodicity *p* of the intensity maxima can be adjusted by positioning of the DOE in the beam bath, which results in a change of the laser beam's incident angle.

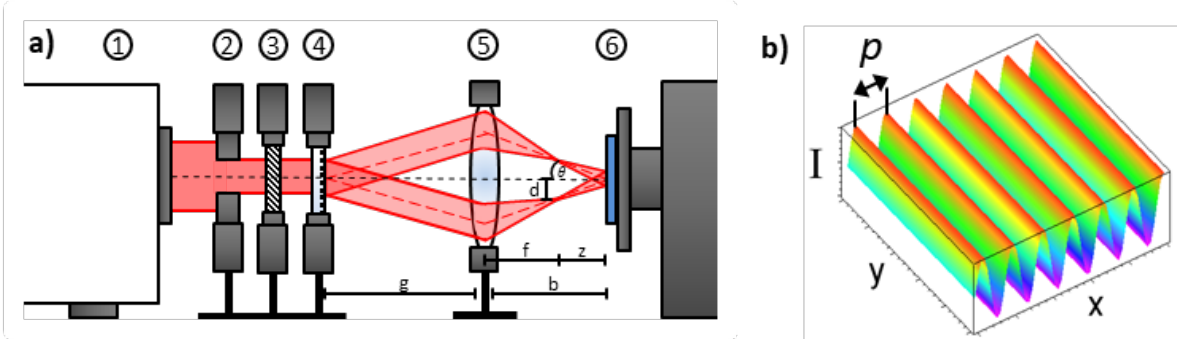

Figure 1: a) schematic illustration of the optical setup for USP-DLIP. 1 laser source, 2 aperture, 3 wave plate, 4 DOE, 5 lens system, 6 automated two axes (x,y) sample mount. b) two beam interference leading to one-dimensional sinusoidal intensity patterns. Periodicity accounts for the distance between two intensity maxima. g is the object distance (1.32 m), b is the image distance (0.11 m), f is the focal length (0.1 m), z is the difference between image distance and focal length (0.01 m), d is the distance of the focal point to the central axis, and θ is the incident angle (2.08 °). Adapted with permission from [38]. Copyright (2020) Springer Nature.

As a result of the high peak intensities, material is ablated at the maxima positions of the intensity distribution, whereas the low intensity at minima positions leaves the material surface largely unchanged. To create continuous patterns the sample is moved using an automated two axes stage, so that the laser scans over the surface of the nanoimprinting tool at a speed of 3 mm/s in continuous pulsing mode with a pulsing frequency of 1 kHz, which results in a hatch distance of 3 µm. For this study the aim was to generate a cross-like surface pattern with closed pockets. To achieve this the surface is processed in two steps, superpositioning two line-like patterns. The first patterning event creates a line-like pattern in y-direction. Subsequently, the nanoimprinting tool is rotated by 90°, and the second patterning event superimposes a line-like pattern in x-direction.

2.2 Materials selection

Tool material

Since the nanoimprinting process is performed on strong metallic alloys at room temperature, it is necessary to ensure that the DLIP pattern on the tool is not damaged during the nanoimprinting process. The tool material should thus be very hard and fracture resistant and furthermore exhibit a very fine-grained microstructure, so that the grain size is smaller than the structures to be created. Ultrafine grained WC-Co hard metals fulfil this requirement, therefore a fine-grained WC-Co hard metal tool (TIGRA GmbH) with a Co content of 10 wt.% and a

grain size of the WC particles of < 1 µm has been used. The chosen alloy has a hardness of 24.2 GPa and a fracture toughness of 10.4 MPa·$m^{1/2}$ [39].

Substrate

Nanocrystalline CuZn30 processed *via* High Pressure Torsion (HPT) was chosen as material to be patterned *via* nanoimprinting. Discs from a CuZn30 brass alloy with a diameter of 20 mm and a height of 2 mm were used for the HPT process at a load of 1400 kN, corresponding to a stress of 4.5 GPa and a total number of 12 rotations. After HPT, the samples had a remaining height of about 1.5 mm resulting in a strain of about 145 at the half radius. Figure 2a shows a TEM micrograph of the material microstructure, with a grain size of about 100 nm. Due to the used process conditions, a steady state saturation grain size is achieved throughout the HPT disc [40]. Moreover, nanocrystalline metals are known for their good mechanical properties. The nanocrystalline CuZn30 alloy used in this study exhibits a flow stress of about 900 MPa (Figure 2 b), thus exceeding the flow stress of most of the commonly used stainless steels. It can therefore be assumed that the nanoimprinting process using a WC-Co tool material can also be transferred to austenitic steels or Ti alloys. Further, Braun and Durst have shown, that CuZn30 shows excellent extrusions properties in a flat punch single contact experiment. In these experiments very high aspect ratios of the produced structures where achieved, with an extrusion height greater than 300 nm at a width of roughly 200 nm [31].

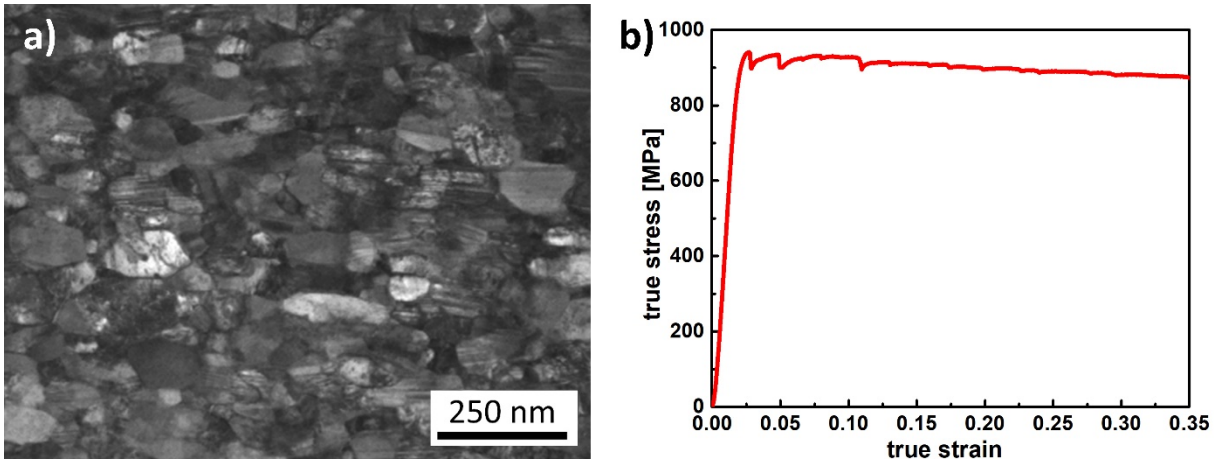

Figure 2: a) Microstructure of the used nanocrystalline CuZn30; b) Stress strain curve in a compression test of the nanocrystalline CuZn30.

2.3 Nanoimprinting

The nanoimprinting tool was fabricated via wire cutting from the WC-Co hard metal, with a shape resembling a flat punch indenter with a diameter of 1.5 mm. The contact face of the tool

was ground and polished (0.25 µm diamond suspension, R_z < 0.01 µm). Afterwards, the tool was fabricated through patterning by DLIP as described in section 2.1. The nanocrystalline CuZn30 substrate was metallographically prepared and polished with an Al_2O_3-suspension (grain size 50 nm) as final step. Before nanoimprinting the substrate was cleaned with ethanol in an ultrasonic bath. Using an Instron 5967 universal testing machine, the patterned WC-Co tool was pressed into the substrate with contact pressures varying between 450 and 3500 MPa (corresponding to a load between 880 and 6200 N) at room temperature. The loading and unloading of the contact were performed in a timeframe between 20 and 60 s. Further development and automatization of the process could possibly strongly reduce imprinting times down to the second range. A schematic representation of the combined process (DLIP and nanoimprinting) can be seen in Figure 3.

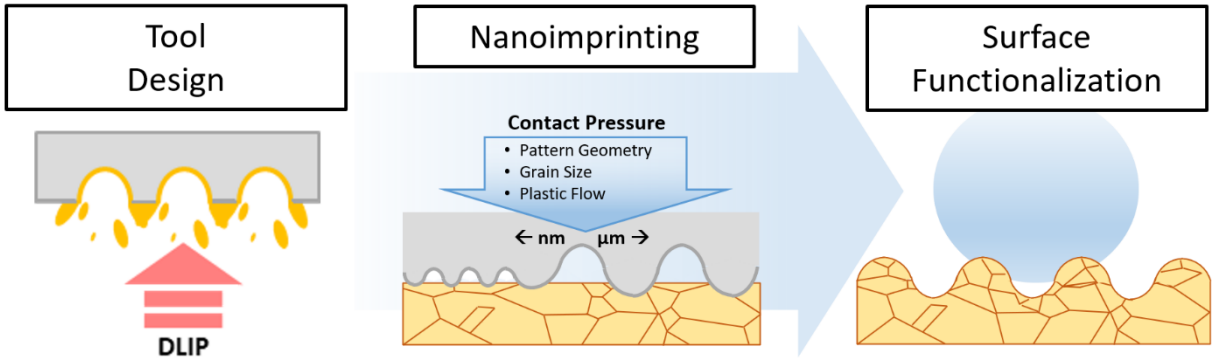

Figure 3: Schematic representation of the combined approach using DLIP for the manufacturing of the tool, which is then used for patterning of the work piece surface via nanoimprinting resulting in its functionalization.

Large-area surface patterns for contact angle measurements were achieved by slightly overlapping individual imprints, resulting in a patterned surface area with a size of about 8 x 11 mm^2. After 10 imprints a cleaning step was carried out using 10%-HCl solution for a period of time of 8 minutes.

2.4 Surface Characterization and Contact Angle Measurement

Scanning Electron Microscopy (SEM, TESCAN MIRA 3, 15 kV and Beam Intensity 10) was used to image the patterns on the tool as well as the patterns transferred to the work piece. To characterize the patterns formed by nanoimprinting, their structure height was measured as the largest difference between the highest and lowest structure features using confocal laser scanning microscopy (LEXT 4100, Olympus). In addition, the arithmetic mean roughness R_a was measured across the whole surface for at least 60 times by averaging line roughness values. To exemplary demonstrate the functionality of nanoimprinted patterns, contact angle measurements with water were performed. The wetting behaviour was characterized with the Contact Angle System OCA (DataPhysics), analysing the static contact angle of a water droplet.

Due to the current technical state with a relatively small patterned surface area of a few square millimetres, a drop of distilled water with a volume of 3 µL was placed on the surface and observed from the side. The water droplet, however, has a diameter of roughly 2-3 mm and covers several thousand nanoimprinted structures. The resulting contact angle is therefore representative for the wetting behaviour of the surface patterns. At least five drops per sample were evaluated and the average was calculated. In addition to the contact angle measurement directly after the nanoimprinting process or the polishing process, the contact angle was measured as a function of the ageing time in dry air at room temperature.

3. Results and Discussion

3.1 DLIP of WC-Co Hard Metal Tool

To investigate the success of laser patterning the WC-Co hard metal tool in terms of pattern homogeneity and surface quality, first, the tool's surface is imaged *via* SEM. As can be clearly seen from the overview Figure 4b, the DLIP pattern is homogeneously distributed over the entire tool surface with a periodic repetition of quasi-identical surface structures, typical for the DLIP process. By using an ultrashort-pulsed laser with a pulse duration in the femtosecond regime, significant heating of the substrate and melt formation can be avoided. Only slight melt residues can be observed on the formed pattern, which are probably generated in the low intensity zones of the pattern [41, 42]. Additionally, no surface damage such as cracks are visible, which is in good agreement with an earlier study on laser processing of a WC-Co substrate, showing less damage during laser patterning with smaller grain sizes [42] which demonstrates the possibility to create high quality laser patterns by DLIP on the WC-Co tool. The width of the produced structures (*i.e.*, the distance between one topographic maximum to the adjacent one) was measured to be 11.3 µm by laser scanning microscopy. The spacing of the ordered patterned surface resembles somewhat the surface of a lotus leaf (Figure 4a), whose primary structures have a spacing in the range of 20 µm, however exhibiting a structure height in the range of 15 µm [43] and a roughness of about 0.6 µm. The DLIP process parameters were adjusted to achieve the largest possible structure height, which resulted in a varying minimum and maximum height of the primary pattern of 2.3 ± 0.1 µm and 4.7 ± 0.1 µm, respectively. This variation of the height can be traced back to the patterning technique, where the crossing points between topographical maxima positions show an even higher structure height by passing over these positions twice, once in x- and once in y- direction. The superordinate pattern is composed of LIPSS, which are clearly visible in Figure 5a. The here observed LIPSS

correspond to low spatial frequency LIPSS as their periodicity of roughly 500 nm (Figure 5a and c) is in the order of the magnitude of the laser wavelength and they are oriented perpendicularly to the laser polarization. As a result of the two-step processing technique the superordinate LIPSS pattern also exhibits a cross-like pattern, which is more pronounced in x-direction, caused by the second laser processing step.

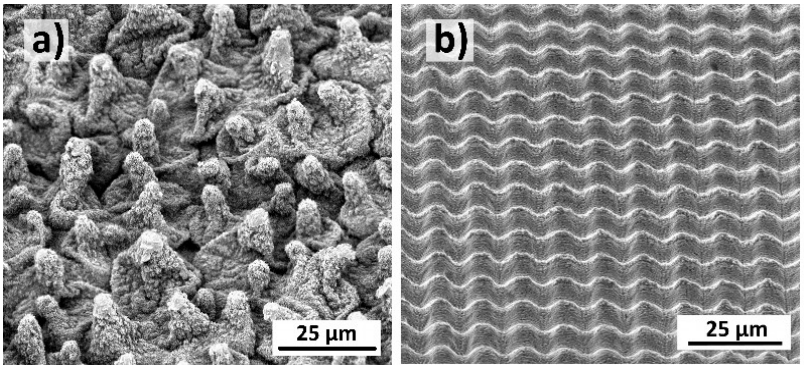

Figure 4: a) SEM picture of the hierarchical surface of a lotus leaf; b) Overview SEM image of the cross-like pattern on the WC-Co carbide tool produced by DLIP with a line width of 11.3 µm.

3.2 Pattern transfer via Nanoimprinting

To generate a pattern on the nanocrystalline alloy having a flow stress in the range of 900 MPa, nanoimprinting experiments have been conducted with varying contact pressures up to a maximum contact pressure of 3500 MPa. After 80 nanoimprinting experiments, no surface damage (*e.g.*, spalling) of the WC-Co tool was found. The surface roughness of the tool is only slightly reduced after all experiments from an initial roughness of 272 ± 70 nm before the experiments to 244 ± 50 nm after the nanoimprinting process (see Figure 5). Nevertheless, some material transfer from the substrate to the WC-Co tool occurs, requiring a cleaning step after ~ 10 imprinting experiments. Future studies will analyse possible wear effects on the tool and their effect on the transferred surface pattern on the substrate.

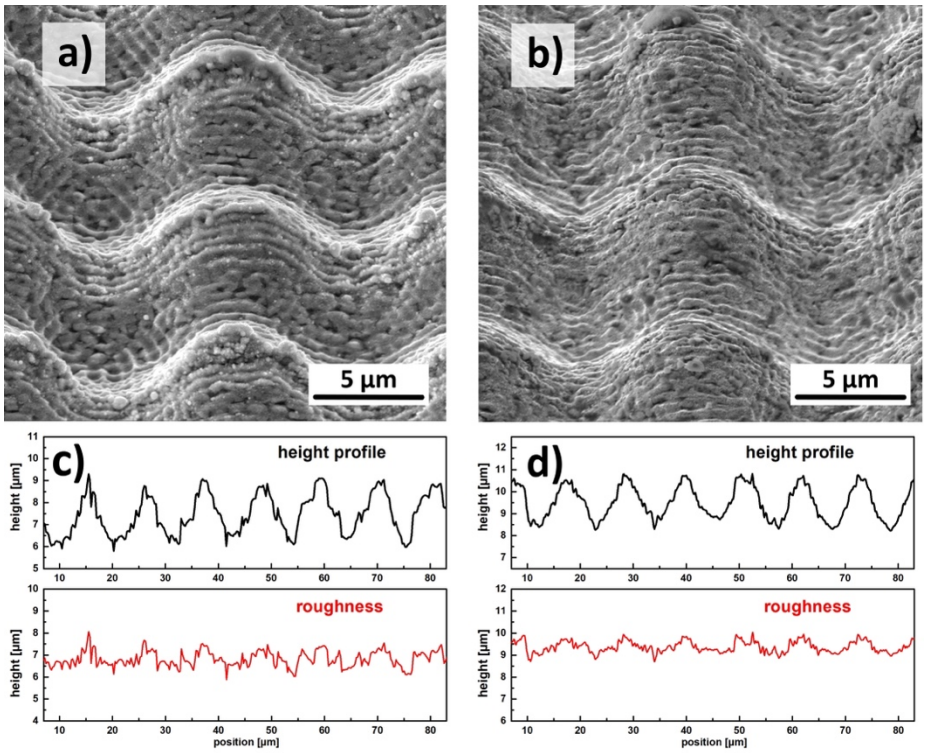

Figure 5: Surface pattern of the WC-Co before (a, c) and after nanoimprinting (b, d). In the SEM images, the LIPSS structure before a) and after imprinting b) is clearly visible. The roughness as well as the height profile after nanoimprinting d) are slightly smoothened in comparison to the initial condition c). However overall, the surface pattern as well as the LIPSS pattern are clearly preserved even after 80 imprinting operations.

Figure 6 gives an overview of the pattern formation at a contact pressure of 2800 MPa. For achieving larger patterned surfaces, imprints were positioned onto the surface with a slight overlap (Figure 6a). In the overlapping areas the pattern is mostly influenced by the last imprint. However, a small step (max. 30 µm) between the single imprints can be seen. The influence of the step height between individual imprints can be neglected for the contact angle measurements, since the contact angle is mainly affected by the contact line rather than the contact area [44]. A close-up of the pattern formed with 2800 MPa on the CuZn30 substrate is shown in Figure 6b. The light grey areas in the laser scanning micrograph correspond to the topographic maxima, whereas the dark areas correspond to topographic valleys, called dimples in the following. The profiles of the created dimples are found in a cross-sectional analysis of the pattern, imaged by 3D laser scanning microscopy (Figure 6d, scan 1). For the applied contact pressure, a maximum structure height of roughly 3.5 µm is achieved. In contrast, when following a profile in x- or y-direction a reduced structure height is found (Figure 6d, scan 2). These two different primary structure heights found on the substrate correspond to the varying structure height on the tool, being a consequence of the patterning technique. In total a plastic indentation depth (sink-in of the whole tool) of ~300 µm is observed. Within the dimples (darker areas in Figure 6b) even the smallest features of the pattern such as the LIPSS are transferred to the sample surface after the nanoimprinting process, which can be clearly seen in

the SEM picture in Figure 6c. This indicates, that every asperity on the tool (roughly 13,000 in total) is acting like a single contact point. The local material flow is thus governed by the shape of the individual asperities as well as the local contact pressure. Interestingly, the material flow is also following the LIPSS pattern, effectively transferring the surface pattern on the tool to the nanocrystalline CuZn30 substrates. The contact situation of the individual asperities on the forming tool resembles the contact situation of nanoimprinting experiments performed in literature, using a flat punch nanoindenter with a diameter of 10 µm and ring-cavities with widths of 688 nm [31]. There, it has been shown that extrusion heights as large as 1 µm at a width of ~700 nm can be achieved on nanocrystalline CuZn30 alloys, while coarse grained alloys did only show limited material flow. The size of a single asperity on our WC-Co tool is quite similar, which applies also to the 0.5 µm widths of the LIPSS, which serve as cavities. During the nanoimprinting process, the LIPSS appear almost completely filled by the substrate material, reaching a height of about 200 nm with sharp edges. It can be assumed that this high degree of resemblance of the imprinted nanostructures to the LIPSS on the tool is only possible due to the high plastic deformability of nanocrystalline metals. This demonstrates that the knowledge gained from single contact experiments can be transferred to the "macroscopic" nanoimprinting process presented here. Beside the grain size and the associated possible deformation processes, the work hardening behaviour plays a major role during surface patterning *via* plastic deformation. With a low work hardening material, like nanocrystalline CuZn30, the plastic zone stays small and deformation is confined to the tool pattern, thus promoting material flow into the tool pattern. A detailed discussion of the deformation processes involved in nanoimprinting and the effect of the grain size can be found in [29–31].
In general, a good surface quality is achieved with a homogenous distribution of surface structures over the whole surface. Additionally, the occurrence of two different primary structure heights and even smallest features in the form of LIPSS, demonstrate an excellent transferability of the patterns from tool to work piece.

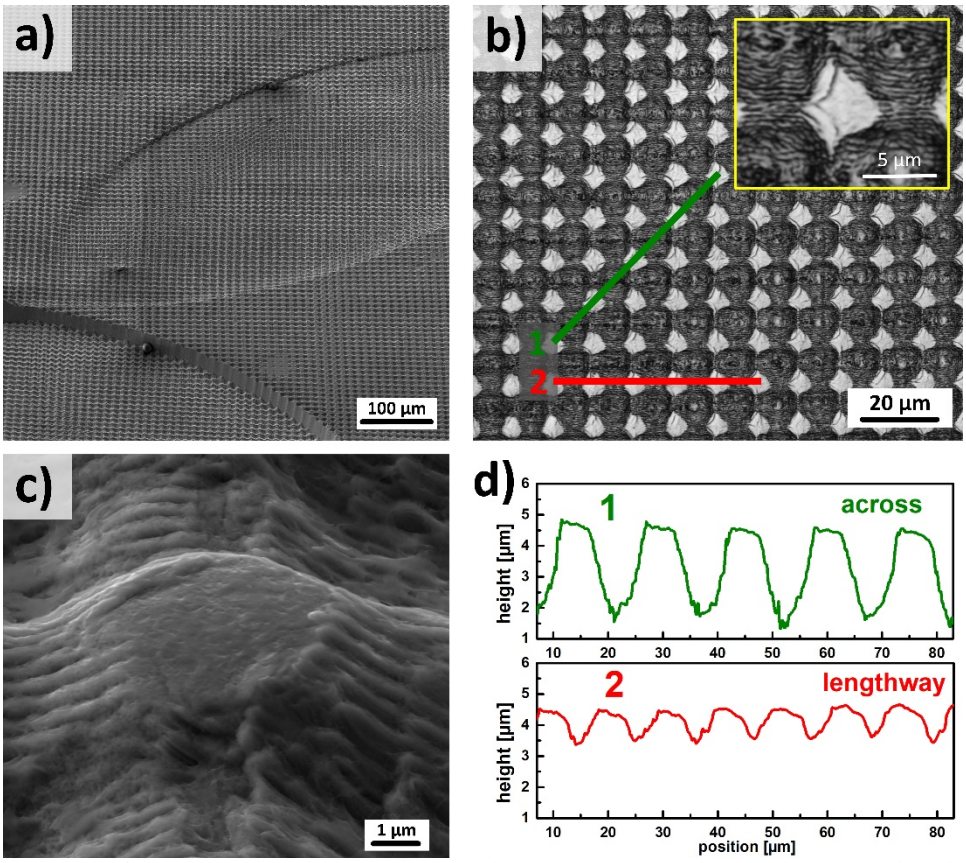

Figure 6: a) SEM scan of the patterned work piece. Three overlapping imprints can be seen. b) Patterned work piece surface (with 2800 MPa) of the nanocrystalline CuZn30 imaged via laser scanning microscopy. The light grey areas are elevated and the dark grey areas correspond to cavities in the surface. The LIPSS structures have also been transferred to the substrate, as visible in the structure of the dark grey areas (cavities). c) SEM picture of the formed pattern under a tilting angle of 55°. The transferred LIPSS on the flanges of the hierarchical structure can be seen clearly. d) Linescans 1) across the pattern, 2) lengthways the pattern. The positions of the scans are marked in b).

To quantify the form filling behaviour, the resulting maximum structure height of the patterned samole as a function of the acting contact pressure as measured from laser scanning microscopy is shown in Figure 7. The data show, that the form filling in terms of structure height linearly increases with increasing contact pressure in the investigated load range. The standard deviation was determined for one structure, at different locations by means of a line profile over at least 10 measured values. The results are minor thus, showing a homogenous manufacturing of the surface pattern with the punches.

At the maximum contact pressure of 3500 MPa, a maximum in structure height of about 4 µm is achieved. However, at this contact pressure the macroscopic indentation depth is about 500 µm. This means that the entire surface underneath the tool is pushed to a level far underneath the initial surface level.

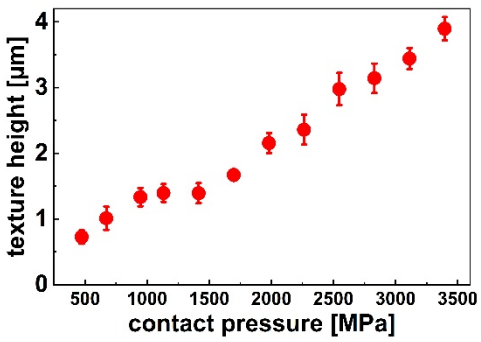

Figure 7: Structure height as a function of the applied contact pressure between tool and substrate, measured at a cross-section via laser scanning microscopy according to Figure 6c "across" configuration.

A detailed analysis of the formed pattern is presented in Figure 8. Height images *via* laser scanning microscopy and the corresponding profiles measured at a cross-section according to the "across"-configuration illustrated in green in Figure 6 b reveal the quality and geometry of the formed pattern on the work piece as a function of contact pressure. For the lowest contact pressure of 470 MPa (Figure 8a), only the highest asperities of the tool are indented into the substrate, forming a homogenous pattern of separated imprinted dimples, which all have roughly the same depth of 800 nm and furthermore, the periodic LIPSS structure is clearly seen within the dimples. As a result of plastic deformation and material flow, small bulges are created at the dimples' edges. Since only the highest asperities of the tool are in contact with the work piece, the surface area between the individual dimples is unchanged and remains flat. Increasing the contact pressure to 2250 MPa (Figure 8b), results in a significant increase of both structure height and width, by a deeper indentation of the tool into the substrate (Figure 8d, note again the LIPSS). At this contact pressure the width of the structures has increased to such an extent that the individual dimples start to contact each other at the edges, thereby forming a chessboard-like pattern of almost square, plateau-like surfaces separated by dimples. Resulting from a higher contact area between tool and work piece and a greater flow of material during the nanoimprinting process, the asperities or topographic maxima positions between the structures get rougher. Finally, for the highest contact pressure of 3500 MPa (Figure 8c), the patterned surface resembles the inverted tool pattern and none of the original surface remains undeformed. The remaining islands (*i.e.*, topographic maxima) start to flow into the cavities of the tool, thereby forming spiky asperities. From now on, a pillar-like pattern with high asperities is achieved. At this applied contact pressure, the pattern on the nanoimprinting tool is almost filled completely by the deformed material (Figure 8d). The process of pattern formation with varying contact pressure can be visualised by superimposing the tool profile (black line) with the surface topography (coloured lines) formed at different contact pressures as shown in Figure

8d. At the smallest contact pressure, only individual separated dimples are formed, whereas increasing contact pressure is initiating plastic flow between asperities. At maximum pressure the profile of the nanoimprinted pattern (dashed pink line) follows the tool profile (black line) quite closely thereby underlining the good transferability of the tool pattern to the substrate at this contact pressure. The results show that significantly different patterns can be achieved with one tool by adjusting the contact pressures and, thus, the introduced plastic flow.

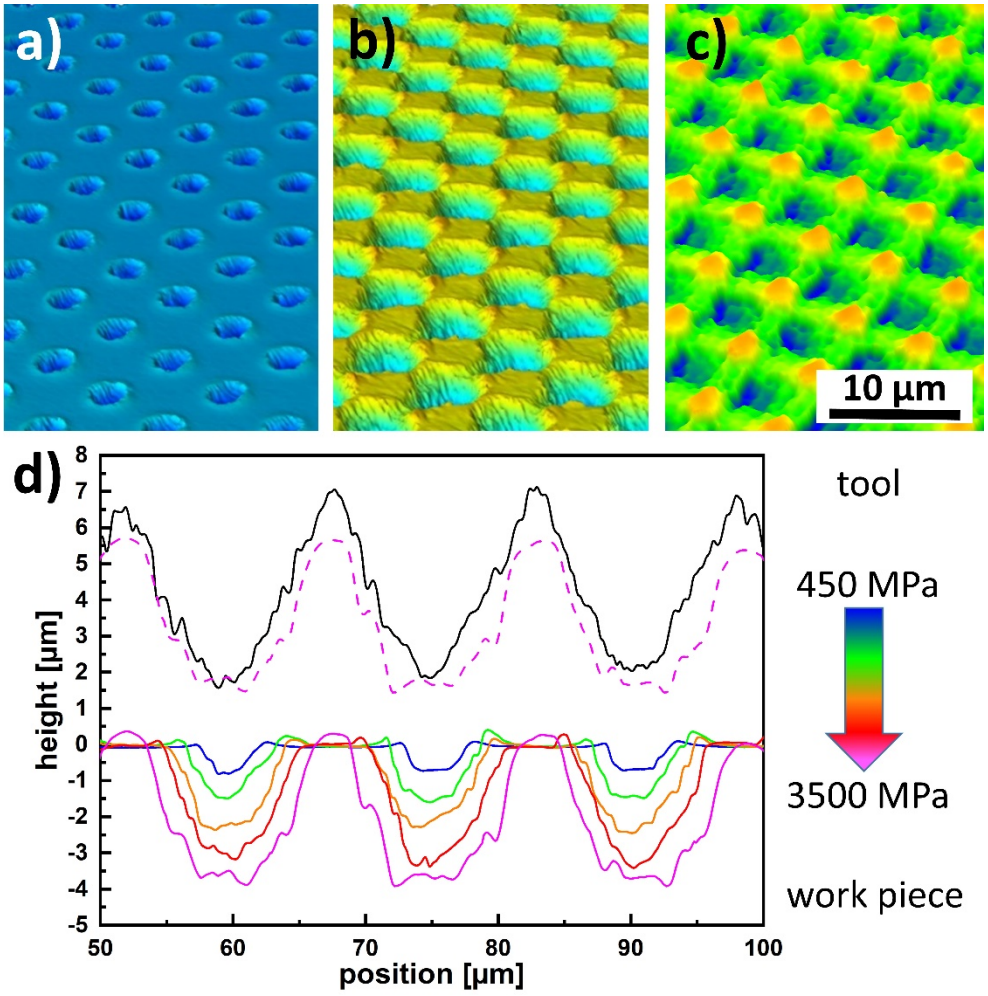

Figure 8: Resulting patterns of the nanoimprinting process with different applied contact pressures of a) 470 MPa, b) 2250 MPa und c) 3500 MPa imaged via laser scanning microscopy. d) Line scans of the used tool (black) and of the formed patterns on the work piece (coloured) with different pressures. The different colours correspond to different contact pressures according to the color-coded legend. The contact pressure for forming the patterns was varied between 470 and 3500 MPa.

3.3 Wetting Behaviour of Nanoimprinted Surfaces – potential application

To demonstrate the effect of surface patterns produced by nanoimprinting on the wetting behaviour of CuZn30 surfaces, contact angle measurements were performed on the patterned surfaces and compared with a polished sample. The measurements were performed as a function of time [45–47]. . Regarding the wetting behaviour two different effects can be

observed, namely a topographical and a chemical one. The topographical effect is induced through a change in structure depth by increasing the contact pressure from 470 MPa to 2250 MPa, whereas the chemical effect results from the accumulation of molecules on the surface due to ageingThe results of the wetting experiments are summarised in Figure 9. Directly after polishing and cleaning with ethanol the polished surface shows a contact angle of 65°, which is a typical value found for polished CuZn30 samples [46]. In comparison, the sample produced with a contact pressure of 470 MPa shows nearly the same contact angle as the polished surface. In contrast, a higher contact pressure of 2250 MPa during the nanoimprinting process leads to a slight increase of the contact angle to 73°. Consequently, directly after the nanoimprinting process a small change of the contact angle (*i.e.*, increase of contact angle by 8°) can be achieved by the use of the nanoimprinted pattern. This decrease in wettability in case of the patterned surface can be correlated with the Cassie-Baxter state, where air is trapped underneath the droplet sitting on top of the dimples [48] or a transition state between Wenzel and Cassie-Baxter state, where the liquid partially penetrates the dimple-like pattern [49]. In contrast to direct laser patterned surfaces no chemical modification of the work piece surface during nanoimprinting is to be expected. The observed effects can be described solely to the influence of the created surface pattern and hence, the modification in surface topography. A comparison of the functionality of patterns manufactured by these two techniques could help in future work to distinguish between the impact of topography and surface chemistry on *i.e.,* the wetting behaviour.

The pattern itself, but also ageing and the resulting chemical processes on the surface, have an effect on the wetting behaviour of metallic surfaces [50]. After ageing the surfaces under dry room air, the contact angles for all measured samples increase. Until an ageing time of 22 days, this increase in contact angle is comparable for the polished surface and the patterned sample nanoimprinted at 470 MPa. Afterwards, the polished sample shows a plateau with stable contact angles around 87° until day 32, whereas the nanoimprinted sample produced at 470 MPa shows a steep increase in contact angle until day 32 resulting in a maximum contact angle of 97°. The sample patterned with a contact pressure of 2250 MPa and thus a greater pattern depth, shows the steepest increase in contact angle with ageing. After an ageing time of 32 days a contact angle of 121° is reached. This time-dependent wetting behaviour was also observed for a variety of laser patterned surfaces in earlier studies and was explained with the decomposition of CO_2 from the atmosphere and an accumulation of nonpolar carbon on the surface [47]. Hence, the influence of ageing on the wetting behaviour can be traced back to the adsorption of molecules on the surface, thereby influencing the surface's chemistry. Therefore, the high contact angles

observed after ageing can be traced back to a synergetic effect of surface patterning and hydrophobization by chemically modifying the surface [47]. In direct comparison with the polished specimen, the patterned specimen reaches maximum contact angles that are around 35° higher. This difference is likely to be dominated by the introduction of a surface pattern through nanoimprinting.

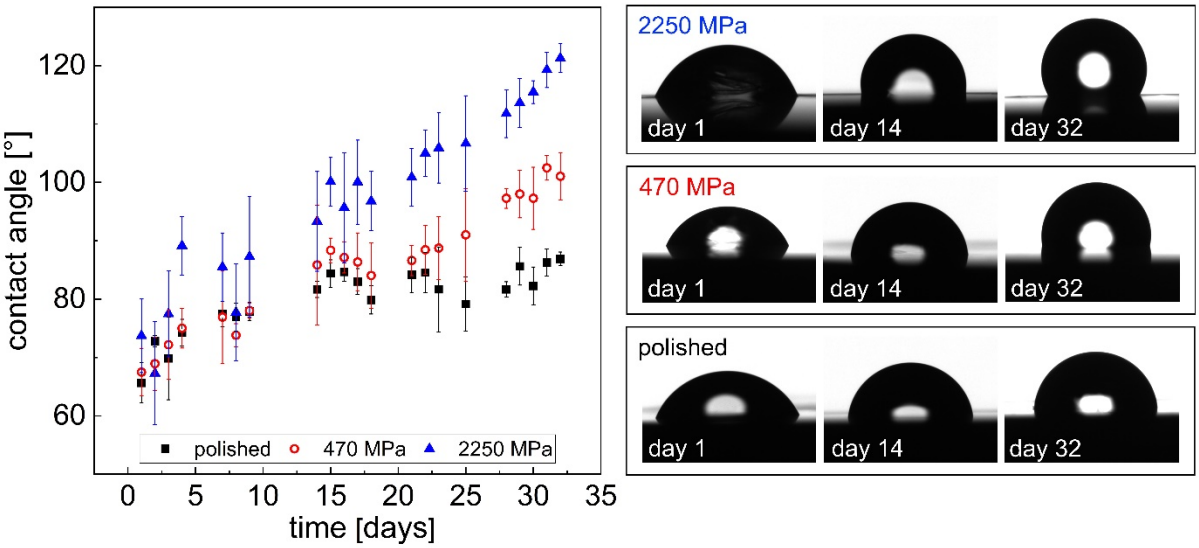

Figure 9: Contact angles of a polished surface and patterned surfaces nanoimprinted with contact pressures of 470 MPa and 2250 MPa as a function of time. In addition, representative images of droplets after different ageing times are shown.

4. Conclusions

In this study, a WC-Co hard metal nanoimprinting tool was laser patterned by Direct Laser Interference Patterning using a femtosecond laser. The patterned tool was used to transfer the patterns to a nanocrystalline CuZn30 substrate by nanoimprinting, applying contact pressures between 0.5 and 3.5 GPa. We investigated the resulting pattern evolution as well as the resulting wetting behaviour of the patterned surfaces. The following conclusions can be drawn:

- The DLIP patterning technique where the laser beam is scanned over the tool surface once in x- and once in y-direction results in a homogeneous cross-like pattern. The primary structures are covered with smaller LIPSS structures, forming a hierarchical surface topography, which has a similar structure spacing as found on lotus leaves.
- In a nanoimprinting process the DLIP pattern is transferred from the tool to an HPT-deformed nanocrystalline CuZn30 work piece. It is particularly interesting that the morphology of the patterns on the work piece can be varied by adjusting the contact pressure, while using the same tool. In this context, the morphology can be tuned to form a surface pattern with separated dimples at low contact pressure or a pillar-like pattern separated by spiky asperities at large contact pressures. After the nanoimprinting process no damage, but only slight smoothening of the tool pattern was observed. We

conclude that a laser patterned tool can be used to introduce plastic deformation into a nanocrystalline metallic surface to reproduce a negative on the tool pattern.

- The samples nanoimprinted with a contact pressure of 2250 MPa showed an influence on the wetting behaviour, increasing the contact angle by 10°, which can be traced back to the topographical effect induced by the patterns. Ageing the samples in dry room air, resulted in a strong increase of the contact angle, in particular for the patterned samples. After an ageing time of 32 days, the sample manufactured at 2250 MPa shows an average contact angle of 121°, while the polished surface shows a contact angle of 87°. The measured contact angle after imprinting is a direct result of the introduced surface pattern, whereas after aging, both pattern and chemical composition influence the wetting behaviour.
- The combination of DLIP and nanoimprinting is a promising approach to create a variety of surface patterns *via* a simple imprinting process without influencing the surface chemistry. The nanoimprinting process can be easily upscaled, making the concept attractive for functionalizing larger metallic substrate areas. Additionally, DLIP-processed tools could be used in machine-hammer-peening to pattern complex geometries.

Acknowledgments

The authors would like to thank PD Dr. Stefan Schneckenburger, Botanical Garden TU Darmstadt, for providing the lotus leaf and Jana Harbig, PtW TU Darmstadt, for the SEM analysing of the lotus leaf, as well as Daniel Müller, Saarland University, for the discussion and schematic representation of the combined approach using DLIP and nanoimprinting. Furthermore, the Deutsche Forschungsgemeinschaft (DFG) is gratefully acknowledged for funding this project (Du 424/9-1).

References

[1] C. Wang, C. Wang, J. Xu, P. Zhang, D. Shan, and B. Guo, “Interactive effect of microstructure and cavity dimension on filling behavior in micro coining of pure nickel,” *Scientific Reports*, vol. 6, no. 1, p. 23895, 2016, doi: 10.1038/srep23895.

[2] T. Shimizu, S. Kosuge, and M. Yang, “Grain size effect on transferability in micro-coining process assisted by ultrasonic vibration,” *Manufacturing Rev*, vol. 2, 2015, doi: 10.1051/mfreview/2015006.

[3] P. G. Grützmacher, F. J. Profito, and A. Rosenkranz, “Multi-Scale Surface Texturing in Tribology—Current Knowledge and Future Perspectives,” *Lubricants*, vol. 7, no. 11, 2019, doi: 10.3390/lubricants7110095.

[4] P. G. Grützmacher *et al.,* “Guiding lubricant on stainless steel surfaces by channel-like structures fabricated by roller- and micro-coining,” *Physica A: Statistical Mechanics and its Applications*, vol. 505, pp. 482–489, 2018, doi: 10.1016/j.physa.2018.03.035.
[5] D. Gropper, L. Wang, and T. J. Harvey, “Hydrodynamic lubrication of textured surfaces: A review of modeling techniques and key findings,” *Tribology International*, vol. 94, pp. 509–529, 2016, doi: 10.1016/j.triboint.2015.10.009.
[6] D. Xia, L. M. Johnson, and G. P. López, “Anisotropic Wetting Surfaces with One-Dimesional and Directional Structures: Fabrication Approaches, Wetting Properties and Potential Applications,” *Adv. Mater.*, vol. 24, no. 10, pp. 1287–1302, 2012, doi: 10.1002/adma.201104618.
[7] A. Rosenkranz, P. G. Grützmacher, C. Gachot, and H. L. Costa, “Surface Texturing in Machine Elements − A Critical Discussion for Rolling and Sliding Contacts,” *Adv. Eng. Mater.*, vol. 21, no. 8, p. 1900194, 2019, doi: 10.1002/adem.201900194.
[8] B. Bhushan and Y. Chae Jung, “Wetting study of patterned surfaces for superhydrophobicity,” *Ultramicroscopy*, vol. 107, 10-11, pp. 1033–1041, 2007, doi: 10.1016/j.ultramic.2007.05.002.
[9] Y. C. Jung and B. Bhushan, “Wetting transition of water droplets on superhydrophobic patterned surfaces,” *Scripta Materialia*, vol. 57, no. 12, pp. 1057–1060, 2007, doi: 10.1016/j.scriptamat.2007.09.004.
[10] D. van Ta *et al.,* “Laser textured superhydrophobic surfaces and their applications for homogeneous spot deposition,” *Applied Surface Science*, vol. 365, pp. 153–159, 2016, doi: 10.1016/j.apsusc.2016.01.019.
[11] D. Wang *et al.,* “Design of robust superhydrophobic surfaces,” *Nature*, vol. 582, no. 7810, pp. 55–59, 2020, doi: 10.1038/s41586-020-2331-8.
[12] D. Quéré, “Wetting and roughness,” *Annual Review of Materials Research*, vol. 38, no. 1, pp. 71–99, 2008.
[13] A. Rosenkranz, L. Reinert, C. Gachot, and F. Mücklich, “Alignment and wear debris effects between laser-patterned steel surfaces under dry sliding conditions,” *Wear*, vol. 318, no. 1, pp. 49–61, 2014, doi: 10.1016/j.wear.2014.06.016.
[14] A. Rosenkranz, T. Heib, C. Gachot, and F. Mücklich, “Oil film lifetime and wear particle analysis of laser-patterned stainless steel surfaces,” *Wear*, 334-335, pp. 1–12, 2015, doi: 10.1016/j.wear.2015.04.006.
[15] C. W. Extrand, “Criteria for Ultralyophobic Surfaces,” *Langmuir*, vol. 20, no. 12, pp. 5013–5018, 2004, doi: 10.1021/la036481s.
[16] N. Michael and B. Bhushan, “Hierarchical roughness makes superhydrophobic states stable,” *Microelectronic Engineering*, vol. 84, no. 3, pp. 382–386, 2007, doi: 10.1016/j.mee.2006.10.054.
[17] B. Bon, J. F. Klausner, and E. Mckenna, “The Hoodoo: A New Surface Structure for Enhanced Boiling Heat Transfer,” *J. Thermal Sci. Eng. Appl*, vol. 5, no. 1, 2013, doi: 10.1115/1.4007439.
[18] Y. Zhu *et al.,* “Surface Structure Enhanced Microchannel Flow Boiling,” *Journal of Heat Transfer*, vol. 138, 2016, doi: 10.1115/1.4033497.
[19] E. Bressan *et al.,* “Nanostructured Surfaces of Dental Implants,” *International Journal of Molecular Sciences*, vol. 14, no. 1, pp. 1918–1931, 2013, doi: 10.3390/ijms14011918.
[20] G. Skrabalak and A. Stwora, “Electrochemical, Electrodischarge and Electrochemical-discharge Hole Drilling and Surface Structuring Using Batch Electrodes,” *Procedia CIRP*, vol. 42, pp. 766–771, 2016, doi: 10.1016/j.procir.2016.02.316.

[21] E. Brinksmeier *et al.,* “Submicron functional surfaces generated by diamond machining,” *CIRP Annals*, vol. 59, no. 1, pp. 535–538, 2010, doi: 10.1016/j.cirp.2010.03.037.
[22] B. Ai, H. Möhwald, D. Wang, and G. Zhang, “Advanced Colloidal Lithography Beyond Surface Patterning,” *Adv. Mater. Interfaces*, vol. 4, no. 1, p. 1600271, 2017, doi: 10.1002/admi.201600271.
[23] W. Li, R. Minev, S. Dimov, and G. Lalev, “Patterning of amorphous and polycrystalline Ni78B14Si8 with a focused-ion-beam,” *Applied Surface Science*, vol. 253, no. 12, pp. 5404–5410, 2007, doi: 10.1016/j.apsusc.2006.12.018.
[24] F. Gottschalch, T. Hoffmann, C. M. Sotomayor Torres, H. Schulz, and H.-C. Scheer, “Polymer issues in nanoimprinting technique,” *Solid-State Electronics*, vol. 43, no. 6, pp. 1079–1083, 1999, doi: 10.1016/S0038-1101(99)00028-3.
[25] L. J. Kricka, P. Fortina, N. J. Panaro, P. Wilding, G. Alonso-Amigo, and H. Becker, “Fabrication of plastic microchips by hot embossing,” *Lab on a Chip*, vol. 2, no. 1, pp. 1–4, 2002, doi: 10.1039/B109775J.
[26] J. Böhm, A. Schubert, T. Otto, and T. Burkhardt, “Micro-metalforming with silicon dies,” *Microsystem Technologies*, vol. 7, no. 4, pp. 191–195, 2001, doi: 10.1007/s005420000084.
[27] C. J. Wang, D. B. Shan, J. Zhou, B. Guo, and L. N. Sun, “Size effects of the cavity dimension on the microforming ability during coining process,” *Journal of Materials Processing Technology*, 187-188, pp. 256–259, 2007, doi: 10.1016/j.jmatprotec.2006.11.055.
[28] Chuanjie Wang *et al.,* “Size effect affected mechanical properties and formability in micro plane strain deformation process of pure nickel,” *Journal of Materials Processing Technology*, 2018.
[29] J. Ast and K. Durst, “Nanoforming behaviour and microstructural evolution during nanoimprinting of ultrafine-grained and nanocrystalline metals,” *Materials Science and Engineering: A*, vol. 568, pp. 68–75, 2013, doi: 10.1016/j.msea.2012.11.056.
[30] K. Durst, S. Hofmann, B. Backes, J. Mueller, and M. Göken, “Microimprinting of nanocrystalline metals – Influence of microstructure and work hardening,” *Journal of Materials Processing Technology*, vol. 210, no. 13, pp. 1787–1793, 2010, doi: 10.1016/j.jmatprotec.2010.06.010.
[31] P. Braun and K. Durst, “A Multiple Length-Scales Nanoimprinting Approach on Nanocrystalline and Strongly Deformed CuZn30 Alloys,” *Scientific Reports*, vol. 10, no. 1, p. 2454, 2020, doi: 10.1038/s41598-020-58874-y.
[32] H. L. Costa and Im Hutchings, “Some innovative surface texturing techniques for tribological purposes,” *Proceedings of the Institution of Mechanical Engineers, Part J: Journal of Engineering Tribology*, vol. 229, no. 4, pp. 429–448, 2014, doi: 10.1177/1350650114539936.
[33] A. F. Lasagni *et al.,* “Direct laser interference patterning, 20 years of development: from the basics to industrial applications,” *SPIE Proceedings*, vol. 10092, p. 1009211, 2017, doi: 10.1117/12.2252595.
[34] F. Mücklich, A. Lasagni, and C. Daniel, “Laser Interference Metallurgy – using interference as a tool for micro/nano structuring,” vol. 97, no. 10, pp. 1337–1344, 2006, doi: 10.3139/146.101375.
[35] Andrés F. Lasagni *et al.,* “Direct laser interference patterning, 20 years of development: from the basics to industrial applications,” in 2017, p. 1009211.

[36] L. Mulko, M. Soldera, and A. F. Lasagni, “Structuring and functionalization of non-metallic materials using direct laser interference patterning: a review,” vol. 11, no. 2, pp. 203–240, 2022, doi: 10.1515/nanoph-2021-0591.
[37] S. Alamri *et al.,* “On the Interplay of DLIP and LIPSS Upon Ultra-Short Laser Pulse Irradiation,” *Materials*, vol. 12, no. 7, 2019, doi: 10.3390/ma12071018.
[38] D. W. Müller, T. Fox, P. G. Grützmacher, S. Suarez, and F. Mücklich, “Applying Ultrashort Pulsed Direct Laser Interference Patterning for Functional Surfaces,” *Scientific Reports*, vol. 10, no. 1, p. 3647, 2020, doi: 10.1038/s41598-020-60592-4.
[39] S. Sheikh *et al.,* “Fracture toughness of cemented carbides: Testing method and microstructural effects,” *International Journal of Refractory Metals and Hard Materials*, vol. 49, pp. 153–160, 2015, doi: 10.1016/j.ijrmhm.2014.08.018.
[40] E. Bruder *et al.,* “Influence of solute effects on the saturation grain size and rate sensitivity in Cu-X alloys,” *Scripta Materialia*, vol. 144, pp. 5–8, 2018, doi: 10.1016/j.scriptamat.2017.09.031.
[41] K.-H. Leitz, B. Redlingshöfer, Y. Reg, A. Otto, and M. Schmidt, “Metal Ablation with Short and Ultrashort Laser Pulses,” *Physics Procedia*, vol. 12, pp. 230–238, 2011, doi: 10.1016/j.phpro.2011.03.128.
[42] S. Fang, C.-J. Hsu, S. Klein, L. Llanes, D. Bähre, and F. Mücklich, “Influence of Laser Pulse Number on the Ablation of Cemented Tungsten Carbides (WC-CoNi) with Different Grain Size,” *Lubricants*, vol. 6, no. 1, 2018, doi: 10.3390/lubricants6010011.
[43] J. Wang, H. Chen, T. Sui, A. Li, and D. Chen, “Investigation on hydrophobicity of lotus leaf: Experiment and theory,” *Plant Science*, vol. 176, no. 5, pp. 687–695, 2009, doi: 10.1016/j.plantsci.2009.02.013.
[44] J. Liu, Y. Mei, and R. Xia, “A New Wetting Mechanism Based upon Triple Contact Line Pinning,” *Langmuir*, vol. 27, no. 1, pp. 196–200, 2011, doi: 10.1021/la103652s.
[45] P. Bizi-bandoki, S. Valette, E. Audouard, and S. Benayoun, “Time dependency of the hydrophilicity and hydrophobicity of metallic alloys subjected to femtosecond laser irradiations,” *Applied Surface Science*, vol. 273, pp. 399–407, 2013, doi: 10.1016/j.apsusc.2013.02.054.
[46] D. Krysciak, S. Rung, and R. Hellmann, “TIME DEPENDANCE OF WETTING BEHAVIOUR AFTER APPLYING LOW SPATIAL FREQUENCY LIPSS WITH THREE DIFFERENT WAVELENGTHS ON BRASS,”
[47] A.-M. Kietzig, S. G. Hatzikiriakos, and P. Englezos, “Patterned Superhydrophobic Metallic Surfaces,” *Langmuir*, vol. 25, no. 8, pp. 4821–4827, 2009, doi: 10.1021/la8037582.
[48] A. B. Cassie and S. Baxter, “Wettability of porous surfaces,” *Transactions of the Faraday society*, vol. 40, pp. 546–551, 1944.
[49] E. Bormashenko *et al.,* “Characterization of rough surfaces with vibrated drops,” *Physical Chemistry Chemical Physics*, vol. 10, no. 27, pp. 4056–4061, 2008, doi: 10.1039/B800091C.
[50] S. M. Lößlein, F. Mücklich, and P. G. Grützmacher, “Topography versus chemistry – How can we control surface wetting?,” *Journal of Colloid and Interface Science*, vol. 609, pp. 645–656, 2022, doi: 10.1016/j.jcis.2021.11.071.